Preparation of Zn-Doped NASICON Electrolyte Material

A Dissertation for
Credits: 16
Submitted in partial fulfillment of Masters Degree

M.Sc in Physics
Goa University
In the subject of Physics

by

Dishant Viturkar
22P0430047

Under the supervision of
Dr. Bholanath Pahari

School Of Physical and Applied Science
Physics discipline

Goa University
May 2024

Seal of the School

Examined by:

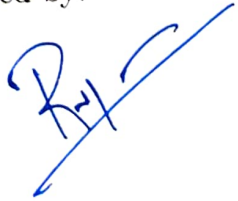

DECLARATION BY STUDENT

I hereby declare that the data presented in this Dissertation report entitled, "Preparation of Zn-Doped NASICON Electrolyte Material" is based on the results of investigations carried out by me in the Physics Discipline at the School of Physical and Applied Sciences, Goa University under the Supervision of Dr. Bholanath Pahari and the same has not been submitted elsewhere for the award of a degree or diploma by me. Further, I understand that Goa University or its authorities will be not be responsible for the correctness of observations / experimental or other findings given the dissertation.I hereby authorize the University authorities to upload this dissertation on the dissertation repository or anywhere else as the UGC regulations demand and make it available to any one as needed.

Name: Mr. Dishant Viturkar

Roll no: 22P0430047

Discipline: Physics

School of Physical and Applied Sciences

Date: 09/05/2024
Place: Goa University

COMPLETION CERTIFICATE

This is to certify that the dissertation "Preparation of Zn-Doped NASICON Electrolyte Material" is a bonafide work carried out by Mr. Dishant Viturkar under my supervision in partial fulfilment of the requirements for the award of the degree of M.Sc in Physics at the School of Physical and Applied Sciences, Goa University.

Supervisor: Dr. Bholanath Pahari

Physics

Date: 09|05|2024.

Dean: Prof. Ramesh. V. Pai

Physics

School of Physical and Applied Sciences

Date:

Place: Goa University

School of Physical and Applied Sciences
Goa University

School stamp

Contents

Chapter 1

Introduction

1.1 Need for Energy Storage Devices

The demand for energy has surged dramatically worldwide due to the growth of industrialization, numerous technological innovations, and economic expansion in developing countries. Consequently, CO_2 emissions have also risen by more than 5% in 2021. To tackle the escalating global environmental issue of CO_2 emissions, renewable energy systems are being implemented at an unprecedented rate since no greenhouse gases or other pollutants are emitted during the process. In 2021, the share of renewable sources in the power generation mix reached a record high of 30%. Notably, solar photovoltaic and wind are estimated to account for two-thirds of renewable growth, with an increase in renewable electricity generation of approximately 18% and 17%, respectively. However renewable sources are intermittent, and energy production can be affected by weather conditions. To address the intermittency and maintain a balance between energy generation and demand, energy storage systems (ESS) are considered the most feasible and effective solution. Energy storage systems are designed to collect energy from various sources, transforming and storing it for various uses.[1]

Electricity is an essential component in modern society, and concerns related

to its availability, cost, and environmental impact are continually discussed in the news. At present most energy is generated from fossil-based sources. The increasing trend in energy production and consumption, along with its negative consequences on air quality, health, and the environment, has shifted the focus towards Renewable Energy Sources (RES). This trend is growing due to scientific, political, and philanthropic interests in creating a sustainable ecosystem, and with it comes the challenges associated with it.

The power system serves as the backbone of the electric energy system, facilitating its production, transportation, and consumption. However, the inherent volatility of Renewable Energy Sources makes energy production and consumption unsustainable. Therefore, managing energy resources requires a sophisticated strategy to maximize the benefits of installed bases and adapt to the changing strengths of production and consumption. Storing electricity appears to be a viable solution to this challenge.

Energy storage in various forms is necessary for the energy system of the future to achieve net-zero targets, ensure reliability and resilience, power quality, electrification of heat and transport, grid modernization, and market coordination. By doing so, energy storage technologies can help alleviate the power system from intermittent production and consumption problems. This in turn, makes energy storage technologies relevant in key application areas such as load shifting, peak shaving, frequency regulation, and others. From an environmental perspective, energy storage increases flexibility and offers solutions to the unpredictable nature of variable renewable energy production curtailment, thereby increasing the system's overall efficiency. From an economic perspective, storage can support deferring transmission and distribution investments, provide better value for existing assets, and reduce costs through energy management.[2]

1.2 History

The progression of a device is highly affected by its general history. A battery or rather an electrochemical cell is a device used for storing and releasing electrical energy that converts chemical energy directly into electrical energy.

The idea that the electrochemical battery was born in the first century BC with the discovery of the "Baghdad Battery" is still believed by some. However, most people now agree that it was Luigi Galvani at the University of Bologna and Alessandro Volta at the University of Pavia in Italy who made the electrochemical cell widely known to humanity at the end of the 18^{th} century.[3]

This significant discovery came about due to a disagreement between the two scientists. Galvani's famous experiment with a frog's leg twitching when touched by different metals led him to believe that animals could generate electricity. Volta, on the other hand, demonstrated electricity production using his "voltaic pile" made up of alternating zinc and silver disks separated by a cloth soaked in a sodium chloride solution.[4]

Although the two discoveries seem to contradict each other, they can be seen as complementary, with Galvani's work related to bio-energy and Volta's to energy storage. Volta's insights about the impact of the electrolyte and electrode interface on electric current flow were remarkable, as they hinted at their critical role in the development of modern batteries, particularly lithium batteries. It's fascinating to read Volta's writings from the late 1700s, where he discusses how the electric current in the pile is not totally free and is hindered by the interruptions between metals, specifically the wet layers that are not good conductors. This anticipates the critical role of the electrolyte and the electrode interface in modern battery development.[3]

1.3 Types of Batteries

Rechargeable batteries are a crucial part of modern life, providing on-demand electrical energy for various applications. In recent years, the increasing demand for better batteries has led to a significant increase in Research and Development efforts. Portable consumer electronics have been the primary driver for this development, but electric vehicles (EV's) and stationary grid storage are now becoming increasingly important. These new applications have different requirements, and no single battery type can meet all of them. As a result, various battery chemistry's are being studied to improve energy density or reduce costs.[5]

1.3.1 Lithium-ion Batteries

Lithium-ion batteries, having profoundly transformed the landscape of energy storage technology, have emerged as the predominant choice for powering a vast array of portable electronics and electric vehicles. Their remarkable energy density, coupled with an extended cycle life and a low self-discharge rate, has propelled them to the forefront of rechargeable battery technologies.

At the core of a lithium-ion battery lies a fundamental architecture comprising a positive electrode (cathode) typically constructed from lithium metal oxides, such as lithium cobalt oxide ($LiCoO_2$) or lithium iron phosphate ($LiFePO_4$). The negative electrode (anode), on the other hand, is predominantly composed of graphite, a form of carbon highly conducive to lithium-ion intercalation. These electrodes are separated by an electrolyte solution, often a lithium salt dissolved in an organic solvent, which facilitates the transport of lithium ions between the two electrodes during the charge and discharge processes.

During discharge, lithium ions migrate from the anode to the cathode, generating a flow of electrons through the external circuit, thus powering the connected device or application. Conversely, during the charging phase, an external power source drives the lithium ions back into the anode, restoring the battery's energy storage capacity.[6]

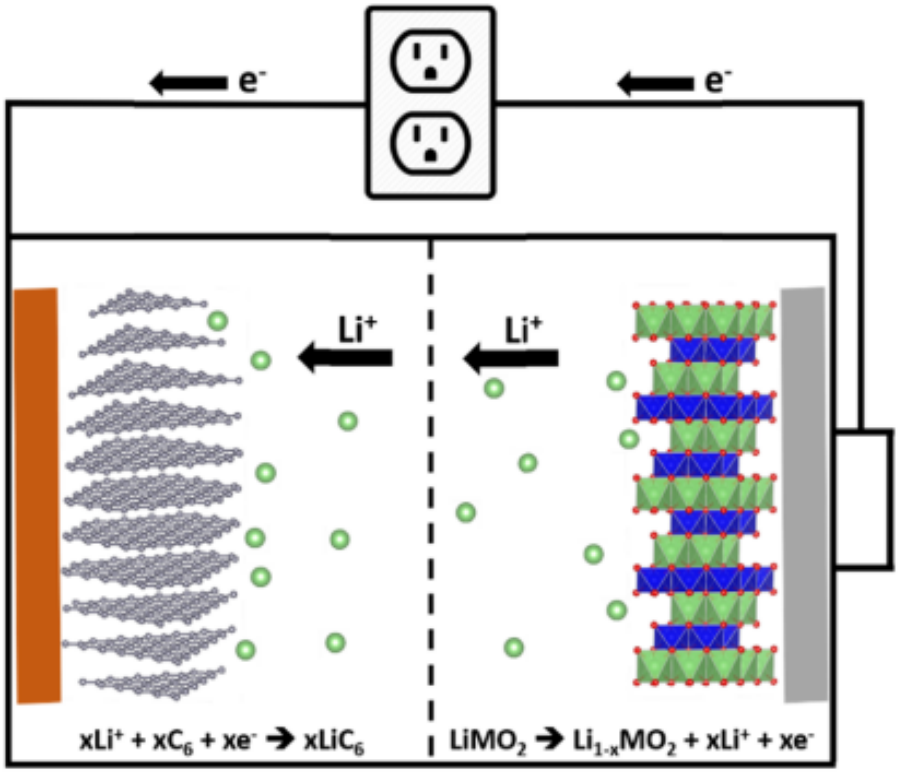

Figure 1.1: Lithium-ion Battery

One of the key advantages of lithium-ion batteries lies in their high operating voltage, typically ranging from 3.6 to 3.8 volts, which translates into a remarkable energy density. This attribute enables these batteries to store a substantial amount of energy within a relatively compact and lightweight package, making them indispensable for portable electronics and electric vehicles, where weight and space constraints are critical considerations.

Moreover, lithium-ion batteries boast an impressive cycle life, often withstanding thousands of charge/discharge cycles before exhibiting significant capacity degradation. This longevity is a direct consequence of the highly reversible intercalation/de-intercalation process of lithium ions within the electrode materials, minimizing structural changes and ensuring long-term stability.

However, like any technology, lithium-ion batteries are not without their limitations. Safety concerns, primarily related to the risk of thermal runaway and potential fires, have been a focal point, particularly in large-scale applications such as electric vehicles. These concerns have prompted extensive research efforts aimed at enhancing safety through the development of more robust electrode materials, advanced electrolyte formulations, and sophisticated battery management systems.

Despite these challenges, lithium-ion batteries have undoubtedly revolutionized the way we power our portable devices and have paved the way for the widespread adoption of electric vehicles, contributing to a more sustainable transportation future.[7]

1.3.2 Solid State Batteries

Solid-state batteries represent a promising next-generation energy storage technology that aims to address some of the limitations of conventional lithium-ion batteries. Unlike traditional batteries that use liquid electrolytes, solid-state batteries employ solid electrolytes, which are typically ceramic or polymer-based materials that can conduct lithium ions.

One of the primary advantages of solid-state batteries lies in their enhanced safety profile. Solid electrolytes are non-flammable and less susceptible to thermal runaway, mitigating the risk of fires or explosions that can occur in liquid electrolyte-based batteries. Additionally, solid electrolytes enable the use of lithium metal anodes, which have a significantly higher theoretical capacity compared to the graphite anodes used in lithium-ion batteries, potentially leading to a substantial increase in energy density.

Furthermore, solid-state batteries offer improved cycle life and coulombic efficiency, as the solid electrolytes are less prone to degradation and side reactions. This translates into longer-lasting batteries with reduced capacity fade over numerous charge/discharge cycles.

However, the development of solid-state batteries is not without its chal-

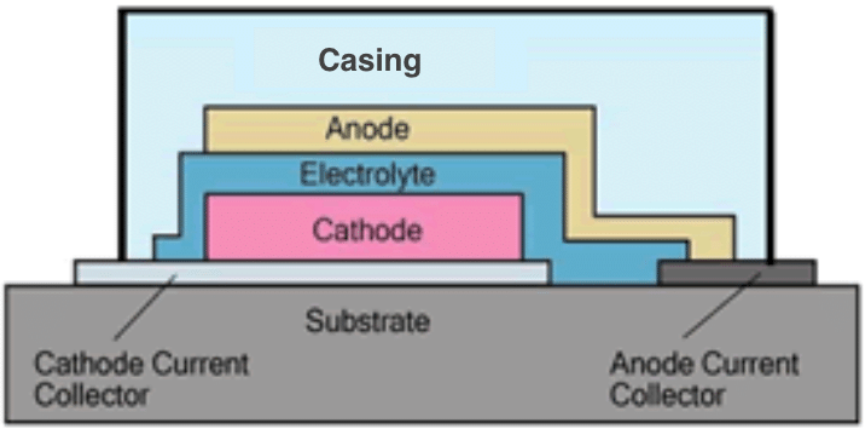

Figure 1.2: Solid state battery

lenges. One significant hurdle is the limited ionic conductivity of solid electrolytes compared to liquid electrolytes, which can result in reduced power density and performance limitations, particularly at lower temperatures. Researchers are actively exploring various solid electrolyte materials, such as sulfides, oxides, and polymer-based electrolytes, to overcome this conductivity issue.

Another challenge lies in the interfacial compatibility between the solid electrolyte and the electrodes. Poor interfacial contact can lead to increased resistance and degradation, hampering the battery's performance and lifetime. Developing effective techniques for fabricating intimate electrode-electrolyte interfaces is an area of active research.

Despite these challenges, solid-state batteries hold immense promise for a wide range of applications, including electric vehicles, grid-scale energy storage, and specialized applications where safety and energy density are paramount concerns. Several major manufacturers and research institutions are heavily invested in solid-state battery research, driving the development of this technology toward commercialization.[8]

1.3.3 Sodium-ion Batteries

Sodium-ion batteries have emerged as a promising alternative to lithium-ion batteries, particularly in applications where cost and resource availability are critical factors. While lithium-ion batteries have dominated the energy storage market, the limited global reserves of lithium and the associated costs have driven researchers to explore more abundant and cost-effective alternatives, such as sodium.

At their core, sodium-ion batteries share similarities with their lithium-ion counterparts, comprising a positive electrode (cathode), a negative electrode (anode), and an electrolyte that facilitates the movement of sodium ions during charging and discharging. However, the choice of electrode materials and electrolyte compositions differs significantly.

One of the key advantages of sodium-ion batteries lies in the abundant availability and low cost of sodium compared to lithium. This factor could potentially lead to a more sustainable and economically viable energy storage solution, particularly for large-scale applications like grid energy storage or electric vehicles for developing economies. Furthermore, sodium-ion batteries exhibit improved thermal stability and safety characteristics compared to lithium-ion batteries. This is due to the inherent properties of sodium-based materials, which are less prone to thermal runaway and potential fires or explosions.

However, the development of sodium-ion batteries faces several technical challenges. One significant hurdle is the lower energy density compared to lithium-ion batteries, primarily due to the larger ionic radius and higher molar mass of sodium ions. This limitation can impact the battery's overall performance and energy storage capacity. [9]

Additionally, the selection of suitable electrode materials that can accommodate the insertion and extraction of larger sodium ions while maintaining structural integrity and high capacity is an ongoing area of research. Commonly explored cathode materials include layered oxide compounds, such as Na_xMO_2 (where M represents transition metals like Fe, Mn, or Ni), while anode materi-

Figure 1.3: Sodium ion battery

als often involve carbon-based structures or alloys capable of reversible sodium storage.

Another challenge lies in the development of electrolytes and separators that are compatible with the sodium-ion chemistry and can facilitate efficient ion transport while ensuring long-term stability and safety.

Despite these challenges, sodium-ion batteries hold significant potential for applications where cost and resource availability are critical factors, such as stationary energy storage systems or electric vehicles targeted at emerging markets. Ongoing research efforts are focused on improving energy density, cycle life, and overall performance, while addressing the remaining technical hurdles. As the demand for sustainable and cost-effective energy storage solutions continues to grow, sodium-ion batteries present an attractive alternative to lithium-ion technology, offering a promising path toward a more diverse and resilient energy storage landscape.[10]

1.4 NASICON

The shortage of top-notch lithium mineral reserves worldwide is holding back the widespread use in big-scale storage systems. High lithium costs are pushing researchers to explore other options, like sodium-ion batteries (SIBs), which could be a budget-friendly alternative for future electric grids since the chemistry of both sodium and lithium is quite similar.

Even though there's way more research on Li-ion batteries than sodium-ion batteries batteries, sodium-ion batteries have been sparking serious scientific interest lately, with research booming in that area. Despite sodium being slower to move due to its size, its abundance and low cost make sodium-ion batteries a solid choice for large-scale use. But when it comes to putting sodium-ion batteries to work using non-aqueous liquid electrolytes, battery safety is a big worry. Those organic solvents in the electrolytes are flammable and not too stable under high heat, which raises major safety red flags, especially in cases of overcharging or internal shorts.[11]

Researchers are looking into solid-state electrolytes (SSEs) as a safer bet because they're rock solid in terms of thermal and chemical stability. Plus, they offer a wider electrochemical potential range compared to liquid organic electrolytes, which means they can be paired with high-voltage cathodes, giving batteries a real energy boost. Solid state electrolytes also simplify battery design by getting rid of the need for a separator to keep the cathode and anode apart.

Still, solid-state sodium-ion batteries are early in their development, mainly because we're still hunting for solid electrolytes with high sodium-ion conductivity and good compatibility with electrodes. The stuff inside solid-state sodium-ion batteries is different from what is in Lithium Ion Batteries, with different materials used for anodes and cathodes.

Solid inorganic electrolytes come in various types for solid-state Lithium Ion Batteries, but for sodium solid-state systems, it's mostly just NASICON, $\beta - alumina$, and sulfides that are used. NASICON stands for Sodium Super Ionic CONductor. Sodium-ion conducting Solid state electrolytes fall into three

categories: polymer-based, sulfide-based, and oxide-based, each with its own pros and cons.[12]

Even though polymer-based electrolytes are flexible and have low resistance, their room-temperature conductivity isn't up to scratch. Sulfide-based electrolytes have achieved decent conductivity and form a solid interface with electrodes, but they're not too stable in normal air conditions, which makes production a bit of a headache. Oxide-based sodium $\beta - alumina$ was the first commercially used superionic conductor, but its high sintering temperature and 2D conductivity make it a no-go for large-scale storage.

NASICON-structured oxides are showing a lot of promise for solid-state sodium-ion batteries, with researchers worldwide eager to develop them as Solid state Electrolytes for sodium-ion batteries operating at room temperature. But there are still hurdles, like the high ionic impedance of NASICON electrolytes and the reactions at the electrode-electrolyte interface, which mess with battery performance.

Solid-state sodium-ion batteries using NASICON ceramic electrolytes are different from Li-based ones. The lower melting point of sodium compared to lithium means it can melt at lower temperatures, which speeds things up. Plus, molten sodium spreads evenly over the ceramic electrolyte, stopping dendrites from forming. Sodium is also softer than lithium, making it easier to handle. And the solid electrolyte is more stable when in direct contact with sodium, since sodium isn't as reactive as lithium. But because sodium ions are bigger, there's a big volume change during charge-discharge cycles, which could mess with battery life. So, keeping a stable electrode-electrolyte interface in Na-Solid State Batteries is trickier than in Li-Solid State Batteries.[13]

NASICON-structured materials, known for their stability, high conductivity, and safety, show great promise for Sodium-Ion Batteries (SIBs). These materials, like $Na_3V_2(PO_4)_3$, are versatile, serving as both anode and cathode. $Na_3V_2(PO_4)_3$, for example, boasts impressive properties: high ionic mobility, a theoretical capacity of around 117.6 mAh g^{-1}, and stable voltage plateaus at 3.4 V and 1.6 V. Similarly, $NaTi_2(PO_4)_3$ is gaining attention for its high capac-

ity, stress-free framework, cost-effectiveness, and thermal stability up to 450^oC. While compounds like $Na_3Zr_2Si_2PO_{12}$ show promising ionic conductivity, they often struggle with slow charge transfer kinetics. To address this, methods like compositing, coating with conducting materials, and doping with cations are explored.

In general, NASICON compounds are represented as AMM, where A can be alkali or alkaline earth metals, or other ions, and M and M sites accommodate various transition metal ions for charge balance. X can be elements like P, Si, S, or As. This flexibility allows for a range of structural arrangements, such as monoclinic, rhombohedral, triclinic, orthorhombic, Langbeinite, Garnet, SW (scandium wolframate) type, or corundum-like.[14]

In this thesis we will be learning of the process and results of synthesising a NASICON solid state electrolyte material with the chemical formula of $Na_{3.2+2x}Zr_{2-x}Zn_xSi_{2.2}P_{0.8}O_{12}$ for x=0 and 0.1. This is a zinc doped NASICON electrolyte which is claimed to have high ionic conductivity which we will be preparing and testing out according to the procedure.

Chapter 2

Experimental Techniques

2.1 Sample Preparation

A NASICON sample with a composition of $Na_{3.2+2x}Zr_{2-x}Zn_xSi_{2.2}P_{0.8}O_{12}$ for x=0 and 0.1 were synthesised and prepared by solid-state reaction. Na_2CO_3, ZrO_2, ZnO, SiO_2 and $NH_4H_2PO_4$ were used in stoichiometric amounts to make 2g of the desired compound and were thoroughly ground into fine powder using a mortar and a pestle and then kept for drying at 80^oC in order to remove excess moisture absorbed by the material when it was stored. These measured powders were taken in a mortar and dry grinding was done such that they are all mixed properly. This was repeated till the powder seemed to be properly mixed and made into a finely ground powder. We then add ethanol and keep on grinding till its dried up giving a fine powder. This is a crucial step in the preparation, the more times this is done the better it is with higher chances of mixing well and lower chances of impurities forming.

Calcination is performed on the sample at 900^oC in a furnace for 10 hours. Grinding was again performed on this calcined powder to make the powder finer and removing any lumps formed. This fine powder is taken and pellets are made using a pellet press which are then sintered in a tube furnace at 1250^oC for 5 hours in air.

For x=0, the compound synthesised was $Na_{3.2}Zr_2Si_{2.2}P_{0.8}O_{12}$. There is no zinc doping in this and we consider it as the Parent compound. The following are the precursors used in their stoichiometric amounts to make 2 grams of the final product.

$Na_{3.2}Zr_2Si_{2.2}P_{0.8}O_{12}$:

Precursors	Amount (g)
Na_2CO_3	0.634
ZrO_2	0.922
SiO_2	0.494
$NH_4H_2PO_4$	0.344

Table 2.1: stoichiometric weights x=0

Similarly for X=0.1, the compound synthesised was $Na_{3.4}Zr_{1.9}Zn_0 \cdot 1\, Si_{2.2}P_{0.8}O_{12}$. This sample is the same as the parent sample doped with zinc. The following are the precursors used in their stoichiometric amounts to make 2 grams of the final product.

$Na_{3.2}Zr_2Zn_{0.1}Si_{2.2}P_{0.8}O_{12}$:

Precursors	Amount (g)
Na_2CO_3	0.672
ZrO_2	0.873
ZnO	0.0304
SiO_2	0.493
$NH_4H_2PO_4$	0.343

Table 2.2: stoichiometric weights x=0.1

These Pellets are sintered and then used for characterization.

For Powder XRD we take the sintered pellet and grind it back into powder form and analyze the powdered sample and conduct XRD on it.

For AC Conductivity and DC Conductivity we take the pellet and coat a layer of silver paste on both sides of the pellet and kept it in an oven for heating at 500^oC for 2 hours. This is done to change the non conducting surface into a conducting one and also because silver is highly thermally and electrically conductive and also provides adhesion.

After this we polish the margin of the pellet such that both the silver pasted sides are not in contact ensuring that the conductivity measurements are accurate and effectively analysed.[15]

2.2 Characterisation Techniques

2.2.1 Powder XRD

In 1912, Max Von Laue and his team stumbled upon a fascinating discovery: when X-rays pass through crystalline substances, they behave like a 3D grid, much like the planes within a crystal lattice. This phenomenon, known as X-ray diffraction, has since become a fundamental tool for exploring crystal structures and the distances between atoms.

X-ray diffraction works by harnessing the constructive interference of monochromatic X-rays and a crystalline sample. These X-rays are carefully generated using a cathode ray tube, filtered to ensure they're all the same wavelength, and then focused onto the sample. When these X-rays interact with the crystal lattice, they create constructive interference, resulting in a diffracted ray, provided the conditions match Bragg's law:

$$n\lambda = 2d\sin(\theta)$$

This equation relates the X-ray wavelength to the diffraction angle and the spacing between lattice planes in the crystal. The diffracted X-rays are then captured, processed, and counted. By systematically varying the angle of the sample, we can capture all possible diffraction directions due to the random orientation of the powdered material. Analyzing these diffraction peaks helps us identify the compound, as each one has a unique set of spacings between lattice planes. This comparison is typically done against standard reference patterns.

A typical X-ray diffractometer comprises three key components: an X-ray tube, a holder for the sample, and a detector for the X-rays. Inside the X-ray tube, electrons are heated to produce a stream, which is then accelerated toward a target. When these electrons hit the target material, they knock inner shell electrons loose, resulting in characteristic X-ray spectra, with common components like K_α and K_β.

K_α, a component of X-ray spectra, is composed of two parts: $K_{\alpha 1}$ and $K_{\alpha 2}$. $K_{\alpha 1}$ has a slightly shorter wavelength and double the intensity of $K_{\alpha 2}$. The specific wavelengths depend on the target material, such as Copper, Iron, Molybdenum, or Chromium. To generate monochromatic X-rays essential for diffraction, filtering through foils or crystal monochrometers is necessary. Since $K_{\alpha 1}$ and $K_{\alpha 2}$ have similar wavelengths, a weighted average of the two is often used. Copper is commonly used as the target material for single-crystal diffraction, with CuK_α radiation having a wavelength of 1.5418Å. These X-rays are focused and directed onto the sample. As both the sample and detector rotate, the intensity of the reflected X-rays is measured. When the geometry of the incident X-rays satisfies Bragg's law, constructive interference occurs, resulting in a peak in intensity. A detector captures and processes this X-ray signal, converting it into a count rate, which can then be outputted to devices like printers or computer monitors.

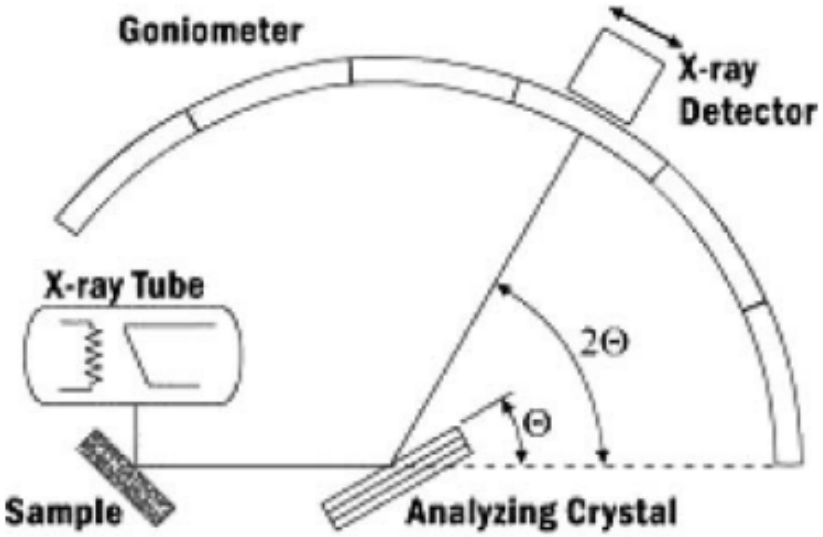

Figure 2.1: XRD setup

In an X-ray diffractometer setup, the sample rotates in the path of the focused X-ray beam at an angle (represented by θ), while the X-ray detector is

positioned on an arm to collect the diffracted X-rays and rotates at twice the angle (2θ). The device responsible for maintaining the angle and rotating the sample is called a goniometer.

During a typical data collection for powder patterns, information is gathered at angles ranging from 5^o to 70^o, represented by θ, which are predetermined in the X-ray scan. X-ray powder diffraction finds widespread use in identifying unknown crystalline materials like minerals and inorganic compounds. Determining the composition of unknown solids is crucial in various fields including geology, environmental science, material science, engineering, and biology. Additionally, X-ray powder diffraction is utilized for characterizing crystalline materials, identifying fine-grained minerals like clays that are challenging to analyze optically, determining unit cell dimensions, and assessing sample purity.

Using specialized methods, X-ray diffraction (XRD) serves various purposes, including determining crystal structures through Rietveld refinement, quantifying mineral amounts, characterizing thin film samples, and assessing textural features like grain orientation in polycrystalline materials.

Powder X-ray diffraction (PXRD) has its strengths and limitations:

Strengths:

- Efficient and swift (usually under 20 minutes) for identifying unknown minerals.
- Typically offers clear mineral identification.
- Requires minimal sample preparation.
- XRD equipment is widely accessible.
- Data interpretation is generally straightforward.

Limitations:

- Best suited for homogeneous and single-phase materials when identifying unknowns.
- Access to a database of standard inorganic compounds is necessary.

- Samples, typically in small amounts, need to be ground into powder form.
- Detection limit for mixed materials is greater than 2% of the sample.
- Indexing patterns for non isometric crystal systems can be complex when determining unit cell dimensions.
- Peak overlap may occur, particularly for high-angle reflections, complicating analysis

X-ray diffraction, a highly advanced and non-destructive method, is used for analyzing a variety of materials like metals, minerals, polymers, pharmaceuticals, ceramics, and more. Its applications span across industries such as microelectronics, aerospace, and power generation. Through XRD analysis, one can identify defects in crystals, assess their stress resistance, texture, size, crystallinity, and other structural characteristics with precision.[16]

Instrumentation

The instruments used for measuring powder diffraction has hardly changed since it was developed back in the late 1940s. One significant update in modern gear is the adoption of a minicomputer for controlling, acquiring, and processing data. A typical diffractometer setup consists of system source F, Soller slits P and RP, sample S, divergence slit D, and receiving slit R. The goniometer's axis is positioned at A.

This setup is known as the Bragg-Brentano parafocusing system, where a beam diverges from a line source F, hits the specimen S, diffracts, and then goes through a receiving slit R to the detector. The distances FA and AR are kept equal. The divergence level is determined by the effective focal width of the source and the aperture of the divergence slit D. Axial divergence is regulated by two sets of parallel plate collimators (Soller slits) P and RP placed between the focus and specimen, and between the specimen and scatter slit, respectively. Using a narrower divergence slit results in less coverage of the specimen at a given diffraction angle, thus allowing for lower diffraction angles where the

Figure 2.2: XRD Machine

specimen appears larger (and larger values of d are achievable). However, this comes with the trade-off of losing intensity.

The selection of the divergence slit, along with its corresponding scatter slit, depends on the range of angles to be included. Whether the slit size should be adjusted for a particular angle depends on the available intensity. Behind the scatter slit, a photon detector, often a scintillation detector, captures diffracted X-ray photons and converts them into voltage pulses. These pulses can then be measured by a rate meter to generate an analog signal on a recorder. By synchronizing the goniometer's scanning speed with the recorder, a diffractogram illustrating degrees 2θ versus intensity is produced.

For quantitative analysis, a timer/scaler is included to measure the integrated peak intensity of selected lines from each component of the specimen. Additionally, a diffracted beam monochromator may be employed to enhance

signal clarity. The diffractometer's output is a "powder diagram," representing intensity against diffraction angle, often presented as a strip chart or a hard copy from a computer graphics terminal.

The term "powder method" originates from the typical form of the specimen, which is usually a microcrystalline powder. However, any material with an ordered atomic arrangement will produce a diffraction pattern. Although the potential of using diffraction patterns for phase identification was acknowledged by 1935, it wasn't until the late 1930s that a systematic approach to deciphering overlapping diffraction patterns was proposed by Hanawalt, Rinn, and Frevel in 1986.[17]

2.2.2 AC Conductivity

Electrochemical Impedance Spectroscopy

Electrochemical impedance spectroscopy (EIS) is a widely used electrochemical technique that measures the impedance, or resistance, in an electrical circuit. Compared to other electrochemical methods, EIS has several advantages:

- It is a steady-state technique, meaning the system being studied is in a stable condition.
- It uses small signal analysis, which means the perturbations applied to the system are small, allowing for linear system analysis.
- It can probe signal relaxations over a very wide range of frequencies, from less than 1 millihertz (mHz) to greater than 1 megahertz (MHz), using commercially available electrochemical workstations (potentiostats).

These features make EIS a powerful tool for studying electrochemical systems and processes, as it can provide detailed information about the electrical properties and behavior of the system under investigation.

Basic Concept of EIS

When it comes to a standard electrochemical cell, the interactions between the matter (redox species) and the electrode involve a few key factors. These include the concentration of the electroactive species, the transfer of charges, and the movement of substances from the bulk solution to the electrode surface, as well as the resistance of the electrolyte. Each of these aspects can be represented by an electrical circuit made up of resistors, capacitors, or constant phase elements connected in parallel or series to form an equivalent circuit.

This equivalent circuit model allows electrochemical impedance spectroscopy (EIS) to be used to explore processes like mass transfer, charge transfer, and diffusion within the system. EIS provides the ability to study the intrinsic

properties of materials or specific processes that can influence the conductance, resistance, or capacitance of an electrochemical system.

One key difference between impedance and resistance is that resistance in direct current (DC) circuits follows Ohm's Law directly, whereas impedance is a more complex measure. In EIS, a small signal excitation is applied, and the system's response is measured. This response is pseudo-linear, meaning the current response is also sinusoidal at the applied frequency, but with a phase shift relative to the excitation signal.

This phase shift is an important characteristic that EIS can analyze to gain insights into the electrochemical processes occurring in the system. The excitation signal is represented as a function of time in an equation provided below with E_t being the potential at time t, E_0 the amplitude of the signal, and ω being the radial frequency.

$$E_t = E_0 . \sin \omega t$$

We figure out the connection between the radial frequency (ω) and the applied frequency (f) using equation.

$$\omega = 2\pi f$$

In a linear system, the signal experiences a phase shift (Φ) and shows a different magnitude compared to I_0.

$$I_t = I_0 \sin(\omega t + \Phi)$$

Therefore, the impedance of the whole system can be obtained from the equation

$$Z = E/I = Z_0 \exp(i\Phi) = Z_0(\cos \Phi + i \sin \phi)$$

Z represents impedance, E stands for potential, I represents current, ω indicates frequency, and Φ denotes the phase shift between E and I. Impedance

is described by both a magnitude, Z_0, and a phase shift, Φ. When the applied sinusoidal signal is plotted against the sinusoidal response signal (I), it forms a "Lissajous Plot". Before modern EIS instrumentation, analyzing Lissajous plots was the sole method for measuring impedance.

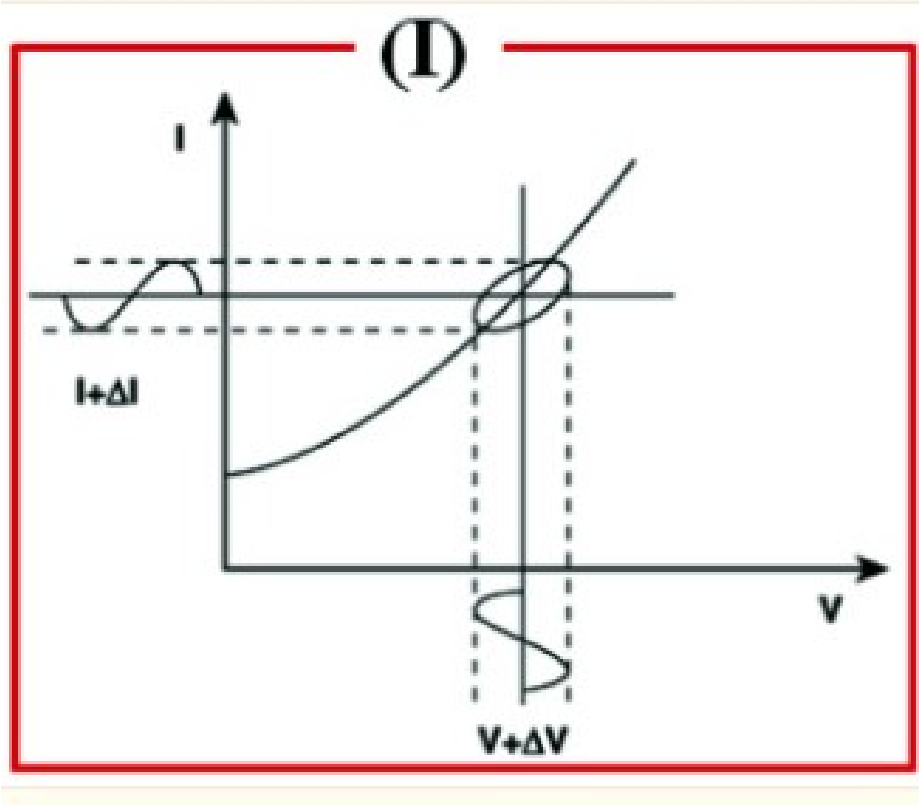

Figure 2.3: Lissajous Plot

Representations of EIS

The impedance expression breaks down into a real portion and an imaginary part. By graphing the real part (Z_{real}) on the X-axis and the imaginary part (Z_{imag}) on the Y-axis, you create what's known as a "Nyquist Plot." Each point on this plot signifies an impedance value at a specific frequency, with Z_{imag} being negative. As you move along the X-axis, impedance at the right side

represents low frequencies, while at higher frequencies, impedance values shift towards the left. Additionally, on a Nyquist plot, you can depict impedance as a vector (arrow) of length —Z—. The angle formed between this arrow and the X-axis is termed the "phase angle."

Alternatively, engineers often utilize what's known as a Bode plot to convey impedance results, which is more prevalent in the engineering community compared to the Nyquist plot. The Bode plot consists of two distinct logarithmic plots: one for magnitude versus frequency and the other for phase versus frequency.

In practical terms, impedance is gauged by applying a voltage wave to the electrode in action and noting down the ensuing current wave. From these two waves, we derive Z, Φ, $Z_{rea}l$, and Z_{imag}, which are then illustrated. The spectrum is built by measuring these parameters across potential waves of varying frequencies.

The inception of electrochemical impedance spectroscopy dates back to 1975, marked by the measurement of slight sinusoidal potential shifts and their corresponding current responses. In a three-electrode setup, an EIS experiment unfolds by maintaining a fixed applied voltage. The resulting solution resistance (R_s), charge transfer resistance (R_{ct}), and Warburg impedance (Ω) are gathered and depicted in Nyquist plots.

Electrochemical impedance spectroscopy (EIS) manifests in two forms: Faradaic and non-Faradaic. Faradaic EIS occurs during redox reactions, while non-Faradaic EIS, grounded in direct current, relies on double-layer capacitance for its electrical characteristics.

The flow of electrons across electrode surfaces translates into Faradaic current, a key component for quantitative analysis. Plotting frequency against phase angle yields a Bode plot, a valuable tool for determining the capacitance of electrochemical systems; for deeper insights into Bode plots, Scully and Silverman offer valuable resources. Generally, Bode plots excel in assessing capacitive systems, while Nyquist plots are preferred for scrutinizing resistive processes.

The overall impedance of a circuit, comprising the sum of individual impedances,

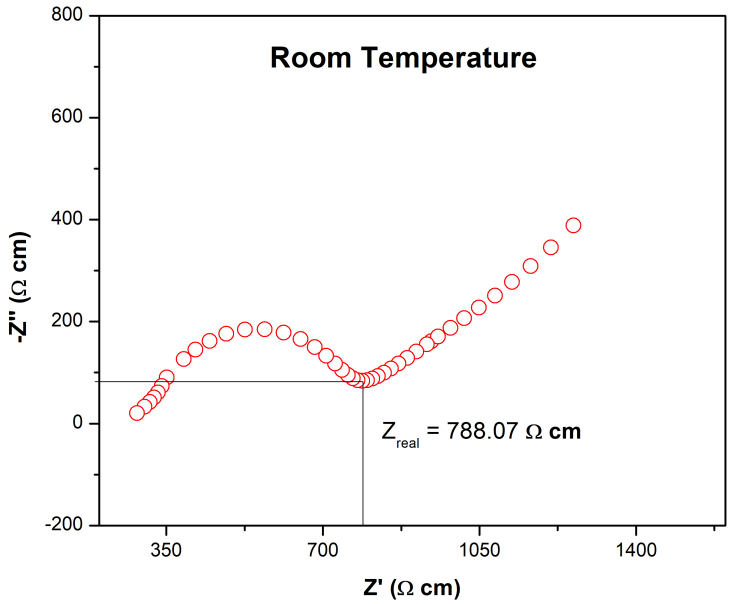

Figure 2.4: Nyquist Plot

is pivotal for analysis. In such scenarios, Ohm's law comes into play, enabling the computation of total impedance across a circuit teeming with various components by summing up the impedances of each element.

$$Z_{total} = Z_1 + Z_2 + Z_3 + \ldots\ldots\ldots\ldots\ldots + Z_x$$

Conversely, the diffusion of molecules or redox species introduces an additional resistance termed the Warburg impedance (Ω). This impedance varies with frequency. Consequently, at higher frequencies, the Warburg impedance remains minimal as diffusing reactants cover shorter distances.

However, at lower frequencies, the force driving redox molecules to diffuse intensifies, resulting in an increase in Warburg resistance. In Nyquist plots, the Warburg impedance of infinity is represented by a slanted line with a 45 ^{o} slope. Similarly, on Bode plots, the Warburg effect is indicated by a 45 ^{o} phase shift.

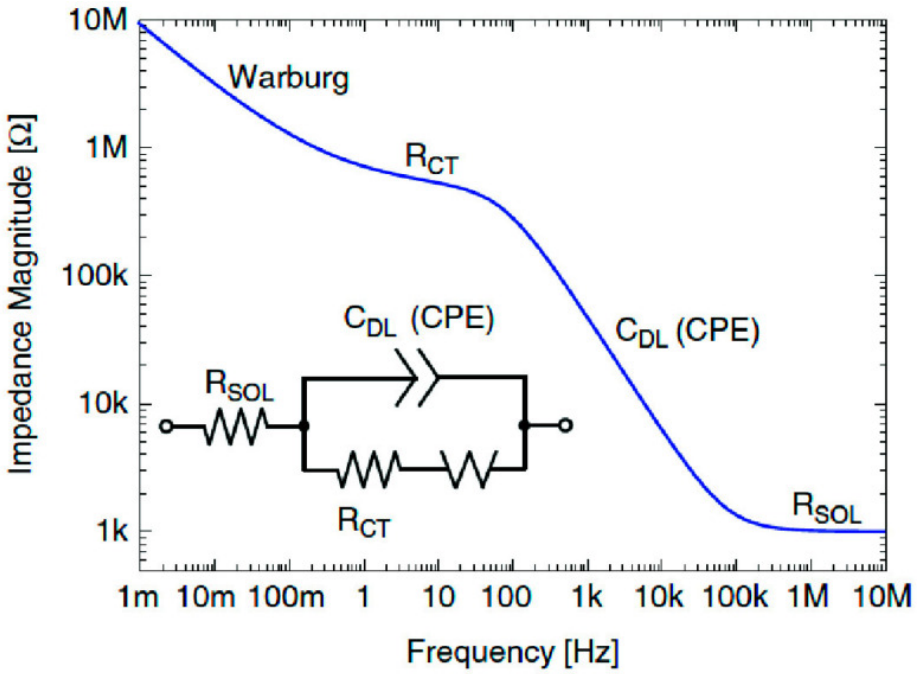

Figure 2.5: Bode Plot

EIS Equivalent Circuits

The electrochemical phenomena linked with electrolyte/interface interactions and redox reactions are replicated through an electrical circuit, known as the equivalent circuit, comprising electrical components like resistors, capacitors, and inductors. This circuit is crafted and utilized to dissect and assess the various elements within the electrochemical impedance spectroscopy (EIS) system.

Parameters such as solution resistance (R_s), double layer capacitance at the electrode surface (C_{dl}), charge transfer resistance (R_{ct}), and Warburg resistance (Z_w) are simplified within Randles equivalent circuits.

Warburg resistance emerges from diffusion processes at the electrode-electrolyte junction. However, the existence of a perfect capacitor in experiments is rare, leading to the incorporation of an additional element termed a constant phase element (CPE) to emulate this non-ideal capacitance behavior. This decision stems from factors like surface roughness, non-uniformity, or porosity of the

materials under investigation.

Nyquist plots, obtained from practical data, aid in identifying and arranging elements of the equivalent circuit based on their Nyquist shape. Thus, acquiring the EIS curve stands as the initial priority, followed by analyzing surface attributes through fitting the electrical circuit simulation. The configuration of a Nyquist plot hinges on factors like the composition of the working electrode matrix and the electrochemical reactions transpiring either at the electrode surface or within the solution bulk. Consequently, diverse Nyquist plot curves may emerge, including single semicircles, two semicircles, or two half-semicircles, contingent on the specific electrochemical operation.

The EIS technique serves as a potent non-destructive tool for characterizing the physical and chemical processes within fuel cells and energy storage devices. Its implementation facilitates the monitoring of stability, performance, and charge transport properties of these materials and devices.[18]

2.2.3 DC Polarisation

Definition

DC polarization is an experimental technique used to study the ionic conduction properties of solid electrolyte and ionic conductor materials. It involves applying a small, constant DC voltage across a sample pellet sandwiched between two different electrodes - one that blocks ions (like graphite) and one that allows ions to pass through (like silver for silver ion conductors).

When the DC voltage is applied, the mobile ions in the sample initially migrate towards the oppositely charged electrode, resulting in a measurable current flow. However, over time, the ions accumulate near the electrodes, forming a depletion or "polarization" region that impedes further ion movement. This causes the current to gradually decay.

Transference Number

Essentially, the transference number provides a way to quantify how much of the total electrical conductivity is due to the movement of ions versus the movement of electrons and holes (the carriers of electronic conductivity). The total conductivity, represented by the symbol σ_{T}, is the sum of the ionic conductivity (σ_{ion}) and the electronic/hole conductivity ($\sigma_{e.h}$).

So we can define the ionic transference number as the fraction of the total conductivity that comes from ionic conduction. Similarly, the electronic transference number is the fraction arising from electrons and holes. By analyzing these transference numbers, we gain insight into the relative contributions of the ionic and electronic charge carrier transport mechanisms to the overall conductivity in the material being studied. This knowledge is valuable for understanding and optimizing properties of ionic and mixed conductors.

$$t_{ion} = \sigma_{ion}/\sigma_T = I_{ion}/I_t$$

$$t_{e.h} = \sigma_{e.h}/\sigma_T = I_{e.h}/I_T$$

The ionic conductivity (represented by σ_{ion}) and the electronic/hole conductivity ($\sigma_{e.h}$) contribute to the overall current flow, with their respective current contributions being I_{ion} and $\text{I}_{e.h}$. The total current (I_T) follows the typical equation: $\text{I}_\text{T} = \text{nqV}_d\text{A}$, where n is the number of charged particles, q is the charge on each particle, V_d is the drift velocity, and A is the cross-sectional area.

To quantify the relative ionic and electronic contributions, we calculate the ionic transference number. This can be done accurately using either the Tubandt method or the Wagner method, which are experimental techniques.

The ionic drift velocity (V_d) can be determined by analyzing the current vs time data from the Wagner method, along with information about the number of charged particles (n) and I_T obtained from techniques like Thermally Stimulated Ionic Conductivity (TIC). By separating the ionic and electronic current components, we gain deeper insights into the charge transport mechanisms occurring within the material under study.

Tubandt's Method

The Tubandt method was pioneered by Tubandt himself as a way to experimentally determine the ionic transference number (t_{ion}) in ionic solid materials. It is based on the principles of Faraday's laws of electrolysis.

The basic setup involves sandwiching the ionic solid between two metal electrodes and applying a DC voltage across it. This causes the positive and negative ions within the solid to migrate towards the oppositely charged electrodes. If the electrode materials are chosen such that the ions can dissolve into them, the mass of the electrodes will change accordingly. By carefully measuring the change in mass of the electrodes, as well as monitoring the total charge passed through an external coulometer circuit, one can calculate the ionic transference number.

In one of his early experiments, Tubandt studied silver iodide (α-AgI) using this method. He packed three cylindrical AgI pellets between silver (Ag) and platinum (Pt) electrodes and applied a DC potential. The mobile Ag^+ ions migrated from the Ag anode towards the Pt cathode. He found that the mass lost by the Ag anode exactly matched the mass gained by the Pt electrode and the adjacent AgI cylinder. This mass change also corresponded perfectly to the total charge measured by the coulometer.

Since the ionic conduction was solely due to Ag^+ ions in this case, the ionic transference number calculated to be exactly 1. This validated that in α-AgI, silver ions are the only charge carriers contributing to the ionic conductivity. Later researchers like Takahashi et al. made some modifications to Tubandt's original cell geometry, but used the same fundamental principles to measure ionic transference numbers in various other fast ion conductor systems.

Wagner's Method

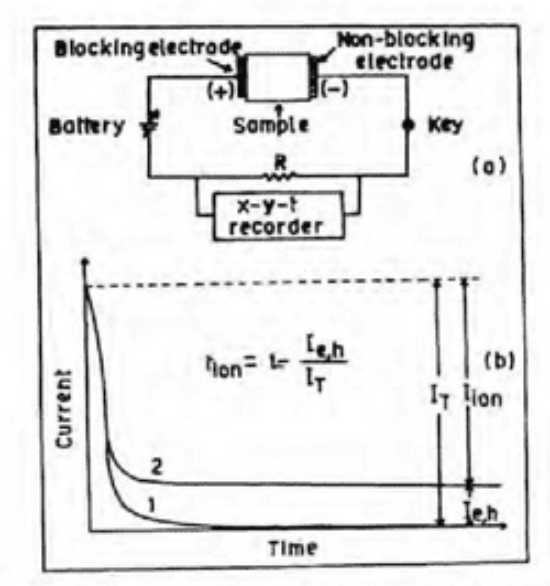

Figure 2.6: Experimental setup

In 1957, Wagner and Wagner proposed a convenient and widely-adopted

experimental method to measure the ionic and electronic contributions to conductivity in solid electrolyte materials. This technique is particularly well-suited for studying silver ion (Ag^+) conductors, which will be the focus here. However, it's worth noting that the same approach can be generally applied to analyse various other solid electrolyte systems as well.

The experimental setup involves preparing a cylindrical pellet of the sample material and sandwiching it between two different electrode materials - one that blocks ions (like graphite) and one that allows ions to pass through (like silver metal). A small DC voltage, typically around 0.5V, is applied across the sample pellet with the indicated polarity. The current flowing through the circuit is then carefully monitored over time using a data acquisition system.

For materials that conduct solely via mobile Ag^+ ions (pure ionic conductors), the total current gradually decays to zero over time. This occurs because the Ag^+ ions fully dissolve into the silver electrode, eventually eliminating the driving force for further ion migration. In such cases, the ionic transference number (the fraction of conductivity from ions) equals unity.

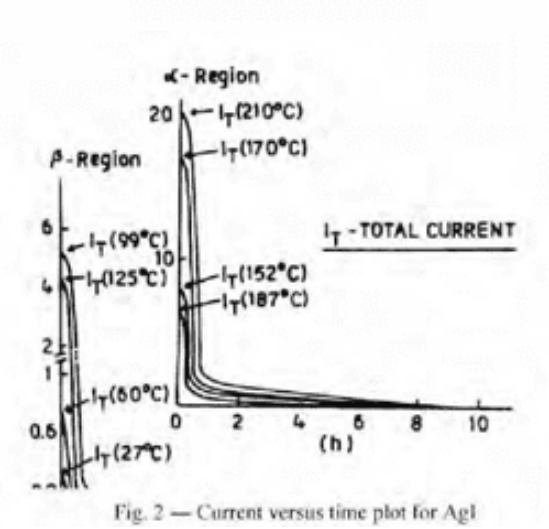

Figure 2.7: Current vs Time Plot

However, if the solid also exhibits some electronic conduction in addition to

ionic conduction (a mixed ionic-electronic conductor), the total current levels off at a non-zero residual value instead of decaying to zero. This residual current arises from the movement of electrons and holes contributing to the overall conductivity. By analyzing the ratios of the ionic and electronic current components to the initial total current, one can quantify the ionic and electronic transference numbers separately.

Interestingly, the current vs time data obtained from Wagner's DC polarization technique can also shed light on the drift velocity of the mobile ions in a purely ionic solid conductor. Let's look at some representative temperature-dependent current vs time plots for the beta and alpha phases of silver iodide (AgI), shown in Regions I and II respectively of Figure 2.2.3. Regardless of the specific material, these plots exhibited some common and insightful trends:

- At all measurement temperatures, the initial total current decayed towards zero over time. This behavior confirms that these materials are purely ionic conductors with Ag^+ ions as the sole charge carriers, resulting in an ionic transference number very close to unity across the entire temperature range studied.

- The polarization time, which is the time required for the total current to essentially reach zero, increased with increasing sample temperature. This makes sense because at higher temperatures, the mobile ions possess more thermal energy and are more agitated, so it takes longer for them to fully polarize and stop migrating under the applied DC voltage, compared to lower temperatures.

- The magnitude of the initial total current also showed an increasing trend with rising temperature.

The increase in the initial total current magnitude with temperature could stem from either an increase in the number of mobile charge carriers (n) or an increase in their drift velocity (V_d). However, if the number of charge carriers

can be independently determined, for example from measurements of the conductivity (σ) and mobility (μ) data, then one can use the initial current values to calculate the drift velocity at various temperatures.

A representative Arrhenius plot of $\log(V_d)$ vs 1/T for silver iodide is shown in Figure 3. Similar plots were constructed for other ionic conductor systems as well. The activation energy (Ed) for this thermally activated drift process was then computed from the straight-line slope in these Arrhenius plots for all the materials studied.

Importantly, it was verified that Ohm's law is obeyed well during these current-voltage measurements. Since drift velocity is directly proportional to mobility at a fixed applied DC field ($V_d = \mu E$), the Arrhenius variations of $\log(V_d)$ vs 1/T and $\log(\mu)$ vs 1/T should be analogous. This means the activation energies E_d and E_μ extracted from the two respective plots must be identical for a given material, reflecting the common underlying thermally activated process.

To further validate the drift velocity measurements, the mobilities were independently determined for all these systems using a complementary technique called Thermally Stimulated Ionic Conductivity (TIC). The drift velocities calculated from the Wagner polarization method were cross-checked against the directly measured mobilities, confirming the validity and self-consistency of this analytical approach.

In summary, the temperature-dependent current transients from Wagner's DC polarization technique provide a convenient way to not only separate ionic and electronic contributions, but also quantify the drift mobility and migration mechanism of the mobile ions in these solid ionic conductors.[19]

Chapter 3

Results

3.1 Analysis by X-Ray Diffraction

The sintered pellets of $Na_{3.2}Zr_2Si_{2.2}P_{0.8}O_{12}$ (parent sample) and $Na_{3.4}Zr_{1.9}Zn_{0.1}Si_{2.2}P_{0.8}O_{12}$ (Zinc-doped sample) which were both prepared by Solid State Reaction were ground into fine powder which was used in XRD analysis. The angle at which the sample was analysed was 10^o to 80^o. The sample was scanned for 10 minutes with a scan rate of 5^o per minute.

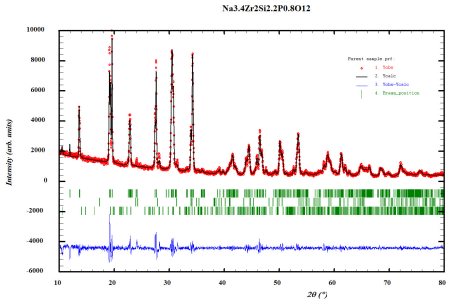

Figure 3.1: XRD of Parent sample

The XRD data was refined using Le Bail Fitting. The major peaks were seen at 20^o, 28^o, 30^o and 34^o with a monoclinic phase with space group C 1 2/ c 1.

Two impurities discovered during refinement of ZrO_2 which is the most common impurity in NASICON materials and $Na_2ZrSi_2O_7$.

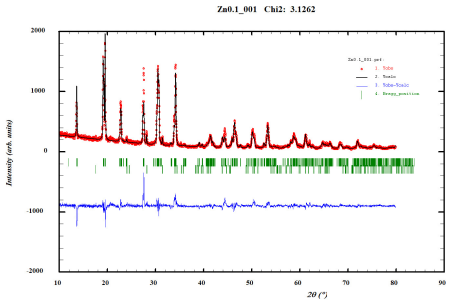

Figure 3.2: XRD of Zinc-doped sample

Similarly XRD data of Zinc doped sample was collected which was refined using rietveld refinement obtaining a χ^2 value of 3.12. The major peaks were seen at 20^o, 30^o and 34^o with monoclinic phase. After refinement impurity of ZrO_2 was found in this sample. From this we also gained the phase fraction with 98.59% of main phase and 1.41% of ZrO_2 impurity phase.

Main Phase	a	b	c	α	β	γ
Parent	15.66 Å	9.06 Å	9.213 Å	90^o	123.79^o	90^o
Zn-doped	15.72 Å	9.091 Å	9.218 Å	90^o	124.059^o	90^o

Table 3.1: Lattice parameters

3.2 EIS Measurements

Figure 3.3: Silver Pasted Samples

The sintered pellets were coated with a silver paste and kept in the oven for heating at 500^{o}C for 2 hours. This is done so that the organic compound in the silver paste which acts as an adhesive gets evaporated as it hinders the ionic conductivity. This is also done to reduce contact resistance.

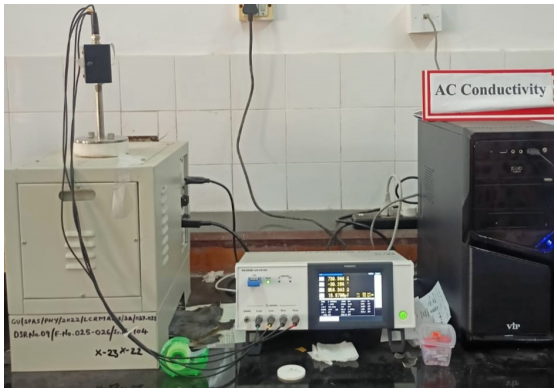

Figure 3.4: AC Conductivity setup

Impedance Spectroscopy was conducted on these silver pasted pellets of $Na_{3.2}Zr_2Si_{2.2}P_{0.8}O_{12}$ (parent sample) and
$Na_{3.4}Zr_{1.9}Zn_0 \cdot 1\,Si_2 \cdot 2\,P_0 \cdot 8\,O_{12}$ (Zinc-doped sample) over a temperature range from room temperature up to 120^oC in order to determine their respective ionic

conductivity at a frequency range of range of $10Hz$ to $9000Hz$. Z(impedance), Frequency and Phase parameter was obtained from the recorded data using which a nyquist plot was plotted.

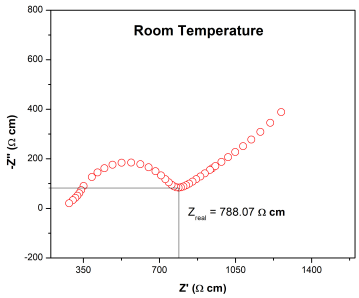

Figure 3.5: Nyquist plot of parent

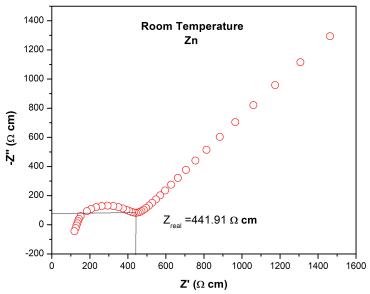

Figure 3.6: Nyquist plot of Zn-doped

Figure3.5 and Figure3.6 are nyquist plots of the samples at room temperature. These graphs were plotted using the formula:

$$Z' = Z\cos(phase(\frac{\pi}{180})(\frac{A}{l})$$

$$Z'' = Z\sin(phase(\frac{\pi}{180})(\frac{A}{l})$$

where A is the area and l is the thickness of the pellet.

The Z_{real} value is obtained from this graph which is the intersecting point of bulk+grain boundary impedance and sample-electrolyte interface. The ionic conductivity was calculated using the formula:

$$\sigma = \frac{1}{Z_{real}}$$

The ionic conductivity of parent at room temperature was observed to be 1.27 $mScm^{-1}$ and for Zn-doped sample, it was 2.26 $mScm^{-1}$. This shows that ionic conductivity increases on zinc doping.

An Arrhenius graph was plotted of $\log(\sigma)$ vs 1000/T using the conductiv-

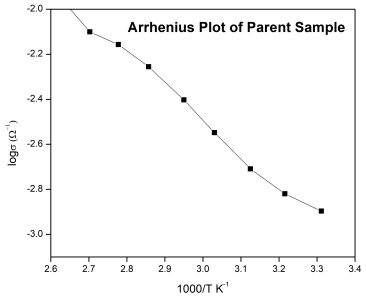

Figure 3.7: Arrhenius plot of parent

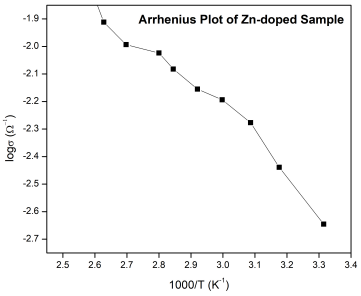

Figure 3.8: Arrhenius plot of Zn-doped

ity's from nyquist plots for temperatures ranging from room temperature up till 120^{o}C. The data showed a trend of a linear rise in ionic conductivity as temperature increases.

3.3 DC Conductivity

Figure 3.9: DC Conductivity setup

DC polarization experiment on the sample was performed, applying 0.8V across it. We recorded the current over time and plotted a Current vs Time graph. Analyzing this plot allowed us to calculate the ionic transference number, giving us the ionic contribution to conductivity.

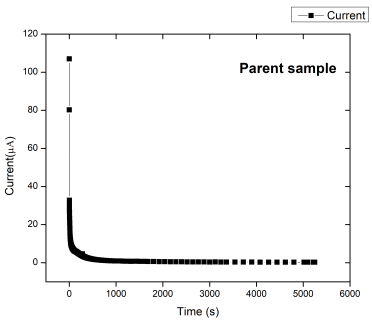

Figure 3.10: DC Conductivity of parent

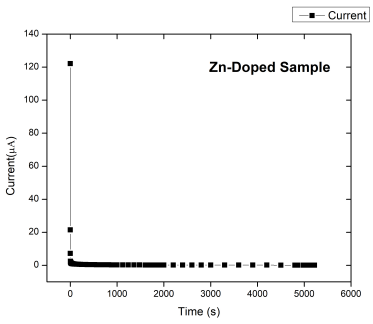

Figure 3.11: DC Conductivity of Zn-doped

The data was recorded for around 5220 seconds. The ionic transference number was expected to be very close to 1. This would essentially mean that nearly all of the electrical conductivity could be attributed to the movement

of ions within the material, rather than being due to the flow of electrons or holes. Materials with ionic transference numbers approaching 1 are considered excellent ionic conductors, with the ions acting as the primary charge carriers facilitating the current flow.

The formula to calculate Transference number is:

$$\text{Ionic Transference Number} = \frac{\text{HighestCurrentValue} - \text{ConstantCurrentValue}}{\text{HighestCurrentValue}}$$

The calculated Ionic Transference Number for parent sample was 0.997 and for the zinc-doped sample was 0.999.

3.4 Conclusion

A NASICON-type solid electrolyte, $Na_{3.2}Zr_2Si_{2.2}P_{0.8}O_{12}$ (NZSP) was synthesized via a solid-state reaction method. Upon doping with zinc, a notable enhancement in ionic conductivity was observed. While the parent NZSP exhibited an ionic conductivity of 1.27 mS cm^{-1}, the zinc-doped variant demonstrated a considerably higher value of 2.26 mS cm^{-1}. Impressively, the ionic transference numbers for the parent and zinc-doped samples were 0.997 and 0.999 respectively, indicating excellent ionic transport characteristics. The reduced grain boundary resistance in the doped material suggests that the addition of zinc aided the sintering process, potentially leading to denser electrolyte materials. This densification could be attributed to improved phase purity and minimal presence of impurities like ZrO_2 and $Na_2ZrSi_2O_7$. The overall decrease in impedance is hypothesized to arise from a synergistic effect – the increased sodium ion concentration coupled with the influence of divalent Zn^{2+} ions on the local structural arrangement within the material. This study highlights the potential of zinc doping as an effective strategy to enhance the ionic conductivity and transport properties of NASICON-type solid electrolytes, making them promising candidates for various electrochemical applications.

Bibliography

[1] J. Mitali, S. Dhinakaran, and A.A. Mohamad. Energy storage systems: a review. *Energy Storage and Saving*, 1(3):166–216, 2022.

[2] Subrat Sahoo and Pascal Timmann. Energy storage technologies for modern power systems: A detailed analysis of functionalities, potentials, and impacts. *IEEE Access*, 11:49689–49729, 2023.

[3] Bruno Scrosati. History of lithium batteries. *Journal of Solid State Electrochemistry*, 15(7):1623–1630, Jul 2011.

[4] A Volta. On the electricity exited by the mere contact of conducting substances of different kind, letter to the right hon. sir joseph banks, kbprs, philos. *Trans*, 2:430, 1800.

[5] Prasant Nayak, Liangtao Yang, Wolfgang Brehm, and Philipp Adelhelm. From lithium-ion to sodium-ion batteries: A materials perspective. *Angewandte Chemie (International ed. in English)*, 57, 06 2017.

[6] Jianmin Ma, Yutao Li, Nicholas S Grundish, John B Goodenough, Yuhui Chen, Limin Guo, Zhangquan Peng, Xiaoqun Qi, Fengyi Yang, Long Qie, Chang-An Wang, Bing Huang, Zeya Huang, Linhui Chen, Dawei Su, Guoxiu Wang, Xinwen Peng, Zehong Chen, Junliang Yang, Shiman He, Xu Zhang, Haijun Yu, Chaopeng Fu, Min Jiang, Wenzhuo Deng, Chuan-Fu Sun, Qingguang Pan, Yongbing Tang, Xianfeng Li, Xiulei Ji, Fang Wan, Zhiqiang Niu, Fang Lian, Caiyun Wang, Gordon G Wallace, Min Fan, Qing-

hai Meng, Sen Xin, Yu-Guo Guo, and Li-Jun Wan. The 2021 battery technology roadmap. *Journal of Physics D: Applied Physics*, 54(18):183001, feb 2021.

[7] George E. Blomgren. The development and future of lithium ion batteries. *Journal of The Electrochemical Society*, 164(1):A5019, dec 2016.

[8] Sevim Aktas, Laura Berkhof, Fergus Collins, Rutger Kersjes, and Annefleur Uitzetter. Solid state battery. 04 2017.

[9] Harshitha B. Tyagaraj, Supriya J. Marje, Kugalur Shanmugam Ranjith, Seung-Kyu Hwang, Amal Al Ghaferi, Nilesh R. Chodankar, Yun Suk Huh, and Young-Kyu Han. Sodium-ion batteries: Charge storage mechanisms and recent advancements in diglyme-based electrolytes. *Journal of Energy Storage*, 74:109411, 2023.

[10] Naoaki Yabuuchi, Kei Kubota, Mouad Dahbi, and Shinichi Komaba. Research development on sodium-ion batteries. *Chemical Reviews*, 114(23):11636–11682, 2014. PMID: 25390643.

[11] Raghunayakula Thirupathi, Vandana Kumari, Sumanta Chakrabarty, and Shobit Omar. Recent progress and prospects of nasicon framework electrodes for na-ion batteries. *Progress in Materials Science*, 137:101128, 2023.

[12] Kushal Singh, Anjan Chakraborty, Raghunayakula Thirupathi, and Shobit Omar. Recent advances in nasicon-type oxide electrolytes for solid-state sodium-ion rechargeable batteries. *Ionics*, 28, 10 2022.

[13] Chi Li, Rui Li, Kaining Liu, Rui Si, Zhizhen Zhang, and Yong-Sheng Hu. Nasicon: A promising solid electrolyte for solid-state sodium batteries. *Interdisciplinary Materials*, 1(3):396–416, 2022.

[14] Ranjusha Rajagopalan, Zhengna Zhang, Yougen Tang, Chuankun Jia, Xiaobo Ji, and Haiyan Wang. Understanding crystal structures, ion diffusion mechanisms and sodium storage behaviors of nasicon materials. *Energy Storage Materials*, 34:171–193, 2021.

[15] Jing Yang, Gaozhan Liu, Maxim Avdeev, Hongli Wan, Fudong Han, Lin Shen, Zheyi Zou, Siqi Shi, Yong-Sheng Hu, Chunsheng Wang, and Xiayin Yao. Ultrastable all-solid-state sodium rechargeable batteries. *ACS Energy Letters*, 5(9):2835–2841, 2020.

[16] Hayat Khan, Aditya S. Yerramilli, Adrien D'Oliveira, Terry L. Alford, Daria C. Boffito, and Gregory S. Patience. Experimental methods in chemical engineering: X-ray diffraction spectroscopy—xrd. *The Canadian Journal of Chemical Engineering*, 98(6):1255–1266, 2020.

[17] Elena gabriela Udrişţioiu Andrei A. Bunaciu and Hassan Y. Aboul-Enein. X-ray diffraction: Instrumentation and applications. *Critical Reviews in Analytical Chemistry*, 45(4):289–299, 2015. PMID: 25831472.

[18] Hend S Magar, Rabeay Y A Hassan, and Ashok Mulchandani. Electrochemical impedance spectroscopy (EIS): Principles, construction, and biosensing applications. *Sensors (Basel)*, 21(19):6578, October 2021.

[19] Rakesh Chandra Agrawal. Dc polarisation : An experimental tool in the study of ionic conductors. *Indian Journal of Pure & Applied Physics*, 37:294–301, 1999.